Volume 1 | Number 1 | Jan 2013 | Pages 1–100

Nanoscale

www.rsc.org/nanoscale

ROYAL SOCIETY OF CHEMISTRY

ROYAL SOCIETY OF CHEMISTRY

www.rsc.org/nanoscale

Cu-Ni nanoparticle decorated graphene based photodetector

Anil Kumar[a,b], Sudhir Husale[a], A. K. Srivastava[a], P. K. Dutta[b], and Ajay Dhar[a*]

[a]CSIR-Network of Institutes for Solar Energy, Division of Material Physics and Engineering,

Council of Scientific & Industrial Research, National Physical Laboratory,

Dr. K.S. Krishnan Road, New Delhi, 110012, India

[b]Chemistry Department, National Institute of Technology, Allahabad 211004,India

----

[*]Corresponding author. Fax: +91 4560 9310.E-mail address: adhar@nplindia.org (Ajay

Dhar)

Abstract

We report a simple and straight forward approach for the synthesis of Cu-Ni graphene hybrid nano-composites. These nano-composites have been characterized by AFM, XRD, FTIR and HRTEM. The characterization data clearly shows a uniform decoration of Cu-Ni nano-particles on graphene layers. A thin film of these nano-composites was found to exhibit unique electrical and photo-response properties, which may be attributed to photo-thermoelectric and photovoltaic effects. The photo-current measurements indicate superior light absorption and a long life time of this device.

1. Introduction

The optoelectronic properties of two-dimensional graphene [1, 2] has fascinated sizeable attention because of its unique band structure, electron-hole symmetry[1] and conversion of photonic energy into photocurrent. Single layer graphene has a capacity to absorb ~ 2.3% of incident radiation over a broad wavelength of light[3]. Moreover, one atom thick nano-materials play a valuable role for its electronic[4], thermal[5], optical[6, 7] and mechanical[8] applications. Hybrid forms of graphene have been used as a foundation for several transformative technologies ranging from energy harvesting[9, 10], biosensors[11, 12], targeted drug delivery[13, 14], flexible microelectronics[15] and electromagnetic interference shielding[16]. Semi-metallic[17] properties of hexagonal honeycomb graphene are useful for nanoelectronics[18] and photon-electron conversion[1] in photovoltaic applications. However, the decoration of metal/alloy on a nanostructured allotrope of carbon can expand their potential use for novel applications[19] such as, gas sensors[20], hydrogen storage[17]and lithium ion battery[21, 22]. It is also proposed that decorated graphene can also play a significant role in photonics[23] due to its enhanced capacity to convert photonic energy into electronic excitation. Multiple evidences in the literature have proved that multiple electron-hole pairs can be created from single photon absorption during the photo-excited operation in decorated graphene derived devices[24]. More recently, Dali Shao et al. have reported zinc oxide nanoparticle graphene core shell based ultraviolet photo-detector with a very good photo-response and photocurrent to dark current ratio[25].

An ideal photosensitive material possesses either good absorption efficiency or long life time of photo-excited carriers[26, 27]. Monolayer graphene derived photo-detectors have low absorption thereby generating very few photo-carriers resulting in poor quantum efficiency. On the other hand, metal nano-particle decorated graphene sheets are known to exhibit metal impurity controlled localisation properties [28, 29], that are expected to influence

the absorption efficiency as well as the life time of generated photocurrent carriers[30]. In optoelectronics, electron-hole pair generation in semiconductor depend on excitation from valance to conduction band, where density of state at Fermi level plays a significant role. In case of metal doped graphene, combined properties of both semiconductor and metal are inherited as its Fermi level is detuned away from the Dirac point[30]. In graphene, the photovoltaic and photo-thermoelectric (PTE) mechanism take place via photocurrent generation at the p-n junction formed near metal graphene contacts, thereby enhancing the hot carriers in the system[31, 32]. Recent studies have observed that secondary hot carrier generation in metal doped graphene occurs via PTE phenomenon, which can be controlled by radiation-induced temperature gradient[33]. In these composites, the presence of disorder in terms of defects, edge roughness and nanostructure considerably reduces the thermal conductivity due to increased phonon scattering[34], vacancies[35] and substitutional impurities[36]. This is an alternate strategy to reduce lattice thermal conductivity of graphene, either by metal/alloy doping or their nanosized decoration leading to increase scattering centers[37] and this phenomenon may promote creation of effective temperature gradient in doped graphene.

Bimetallic composites possess very exciting physical as well as chemical applications[38]. Cu-Ni alloy as such possess some exciting properties[39], like, low temperature coefficient of expansion, low electric resistivity, thermoelectric property, good corrosion and wear resistance etc. Theoretical evidences have shown that Ni has good cohesive energy, strength and electronic structure, which can be correlated directly with graphene atomic geometry[40]. On the other hand, Cu has better electrical, thermal and optical properties compared to Ni. The hybrid nature of both the elements combined together with graphene, may turn out to be more suitable metal-graphene nano-composites for advanced optoelectronic applications.

In the present study, we demonstrate the synthesis, morphological characterization, electrical and photo-sensitive response of Cu-Ni nano-particles decorated reduced graphene sheets. The fabrication process employed is economical, fast and reproducible, wherein the synthesis of Cu-Ni (Cu/Ni ratio 1:1, please see supplementary Fig. 2S) nano-particles and its decoration on graphene takes place in situ. Simple chemical reduction chemistry has been used for this purpose, where ammonia acts as complexing agent and hydrazine hydrate as a reducing agent[41]. We investigate the photo-response of Cu-Ni graphene hybrid nano-composite in presence of white light (halogen lamp) as a photodetector. This hybrid nano-composite shows improved light absorption and enhanced life time of photo-excited carriers.

2. Experimental

2.1 Materials

Graphene oxide (GO), used in the present study, was prepared in-house (CSIR-NPL, New Delhi). Graphite powder (Ultra carbon, 99.99%) was used as a starting material to obtain GO by using modified Hummer's method[42]. Chemicals, namely, copper sulphate ($CuSO_4.5H_2O$), nickel chloride ($NiCl_2.6H_2O$), ammonia water and hydrazine hydrate ($NH_2NH_2.2H_2O$, 99.99% pure) were procured from Merck, India. This is a fast and simple technique to fabricate the device rather than other expensive methods, but using this technique it is very difficult to control the number of graphene layers for a direct comparison with other similar devices.

2.2 In-situ synthesis of Cu-Ni nanoparticles on graphene oxide by electroless technique

A homogeneous mixture of $CuSO_4.5H_2O$ and $NiCl_2.6H_2O$ (molar ratio 1:1, 0.5g each) was prepared in de-ionized (DI) water with constant stirring at room temperature. Solution of liquid ammonia was added as a complexing agent in the above mixture to form a complex of copper $[Cu(NH_3)_6]^{2+}$ and nickel $[Ni(NH_3)_6]^{2+}$ and stirring was continued. In this mixture,

dispersed GO was added and the temperature was maintained to ~ 60-70°C.   Hydrazine hydrate (10ml) was then added as a reducing agent[41] to form reduced graphene (r-graphene) and r-graphene was allowed to interact with Cu and Ni complexes.   This reaction was allowed to continue (~2hrs) for the growth of Cu-Ni nano-particle on r-graphene surface. The resulting Cu-Ni nano-particles decorated r-graphene hybrid nano-composite (referred as Cu-Ni GrHNC in subsequent discussion) and r-graphene (as such) was used for further characterization.

2.3 Device fabrication for electrical and photoconductivity measurements

A drop casting method was used to form a thin film of Cu-Ni GrHNC on SiO_2 substrate. First, SiO_2 substrate was cleaned and heated to 120°C on hot plate. Drops of Cu-Ni GrHNC suspended in ethyl alcohol were deposited and allowed to evaporate in a fume hood for 20-30 minutes[43]. Silver paste was used to make source and drain contacts on this film for electrical and photoconductivity measurements.

2.3 Material Characterization

Phase identification and crystallite size measurements were carried out by X-ray powder diffraction (XRD) (Rigaku, MiniFlexII) and Fourier Transform Infra-Red Spectroscopy (FTIR, model Nicolet-5700).   The surface morphology was studied using Atomic Force Microscopy (AFM, model Multimode-V, VEECO).   High resolution imaging was done using transmission electron microscope (TEM, FEI, Tecnai T30) to investigate the microstructural characteristics and crystallographic orientation.   A film of r-graphene and Cu-Ni GrHNC was also prepared using drop casting method on quartz slide for Raman analysis (Macro Raman, Renishawin Via) with 514 nm laser for excitation. The photo-response and electrical characterization of Cu-Ni GrHNC under dark and white light (halogen lamp) were carried-out using Keithley-2400 source meter.

3. Results and discussions

6

The synthesis mechanism of Cu-Ni GrHNC has been schematically shown in Fig.1. The AFM image of synthesized GO (see Fig. 2A) shows a topographic height of 0.83 nm, suggesting that it comprises of about two graphene layers[44]. Fig. 2B shows the atomic scale HRTEM image of r-graphene with inter-planar spacing of 3.1Å. Inset of Fig. 2B shows the TEM image of single, double and triple layered r-graphene (marked by arrows). The X-ray diffraction patterns of synthesized GO, r-graphene and Cu-Ni GrHNC are plotted in Fig. 2C. The hump observed in GO at $2\theta = 20-30°$ clearly indicates the presence of nanosized hexagonal graphene. An additional peak at $2\theta=12°$ marks the existence of GO which disappears in case of r-graphene, thereby confirming complete conversion of GO to r-graphene. The characteristic peaks representing FCC structure of Cu-Ni alloy are seen at $2\theta = 43.74°, 50.99°, 75.03°$ with a crystallite size of ~ 11nm (calculated using Hall-Williamson techniques with 111, 200, and 220 planes)[45].
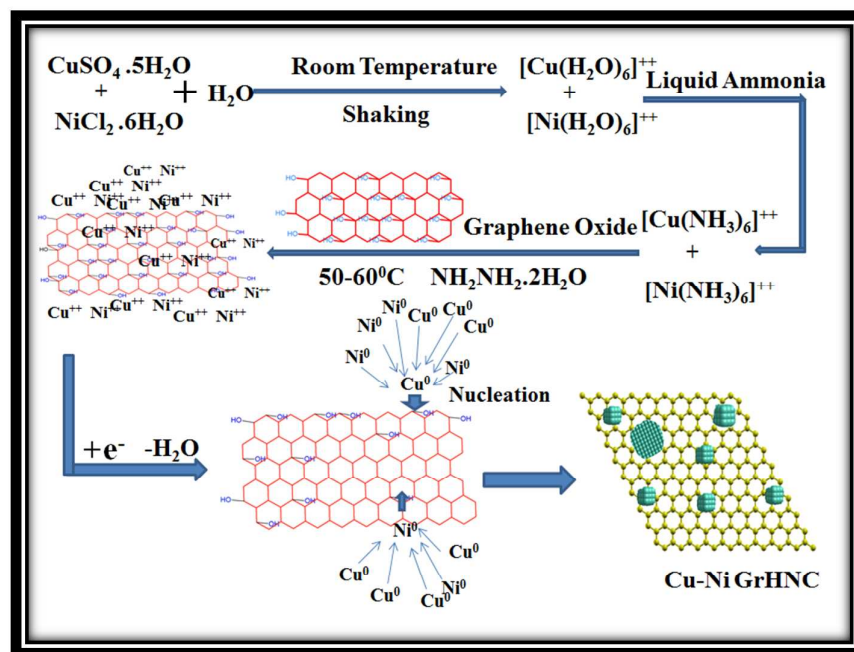
Figure 1: Schematic showing mechanism for synthesis of Cu-Ni nano-particle decorated reduced-graphene hybrid nano-composite (Cu-Ni GrHNC)

The Fig. 2D shows the FTIR spectra observed for GO, r-graphene and Cu-Ni GrHNC. In case of GO, the peaks at position 865, 1038, 1623, 1711, and 2923 cm^{-1} corresponds to -C-H, -C-O-C-, C=C- (for aromatic), -C=O (α,β unsaturated keton) and –C-H (cycloalkane), respectively (marked in the figure). However, for r-graphene and Cu-Ni GrHNC no such additional peaks were observed suggesting that the chemical reduction removes most of the prominent functional groups[41].
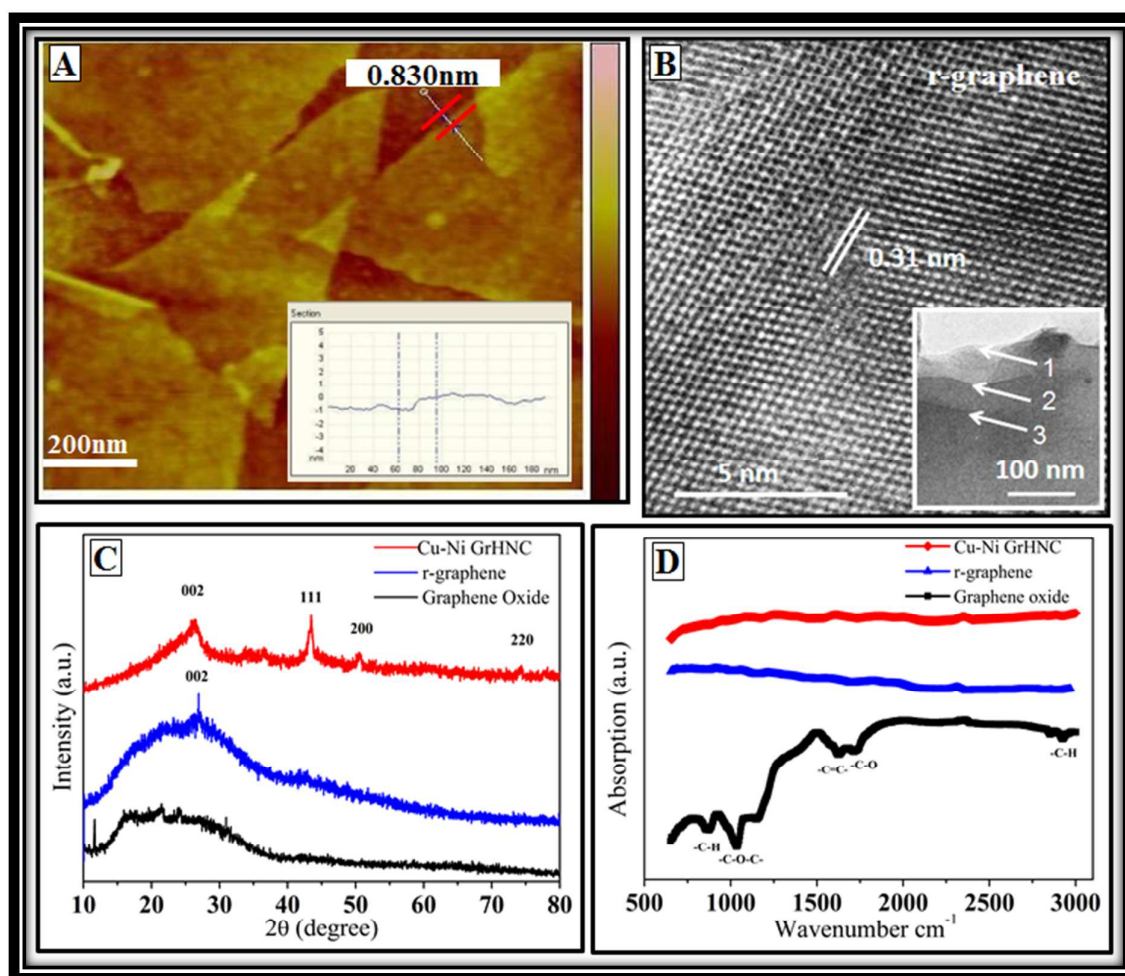
Figure 2 : (**A**) AFM image of graphene oxide (GO) and height profile (inset); (**B**) HRTEM of reduced graphene (r-graphene) and its low magnification TEM (inset) indicating three layers of graphene; (**C**) X-ray diffraction patterns and (**D**) FTIR spectra observed for GO, r-graphene and Cu-Ni GrHNC

The crystallographic structure of Cu-Ni GrHNC was determined by TEM and these microstructures are shown in Fig. 3A. The inter-planar spacing of r-graphene and Cu-Ni alloy are observed to be 3.1 and 2.1 Å, respectively, as seen from the atomic scale image (Fig. 3A) of Cu-Ni GrHNC. The size of the Cu-Ni nano-particles was observed to be around 8nm. The selected area electron diffraction (SAED) pattern, shown in the left inset of Fig. 3A, reveals that the entire plane is a single crystalline hexagonal lattice with 110 planes of graphene and the corresponding ring patterns are generated due to polycrystalline Cu-Ni nano-particles. The low magnification TEM image (right inset of Fig. 3A) depicts a dense network of Cu-Ni nano-particles uniformly decorated on r-graphene.

The physical and chemical nature of Cu-Ni GrHNC and r-graphene, investigated by Raman spectroscopy, are shown in Fig. 3(B-C). Two prominent bands were observed in both spectra at 1587 cm^{-1} and 1354 cm^{-1} corresponding to G and D band, respectively, confirming the presence of graphene derived carbon material. It can also be inferred from this figure that the intensity ratio (I_D/I_G) decreases from 1.63 for r-graphene to 1.45 for Cu-Ni GrHNC. This may perhaps be due to the electron doping in graphene honeycomb structure, which is responsible for local defects and disorder, thereby creating an effective change in E2g photon corresponding to sp2 atoms (G band) and κ-point photon of A1g symmetry (D bands)[46]. Raman shift peaks at 2697 cm^{-1} (2D band) and 2940 cm^{-1} (D + G band) indicate a complete reduction of GO[47] into r-graphene.
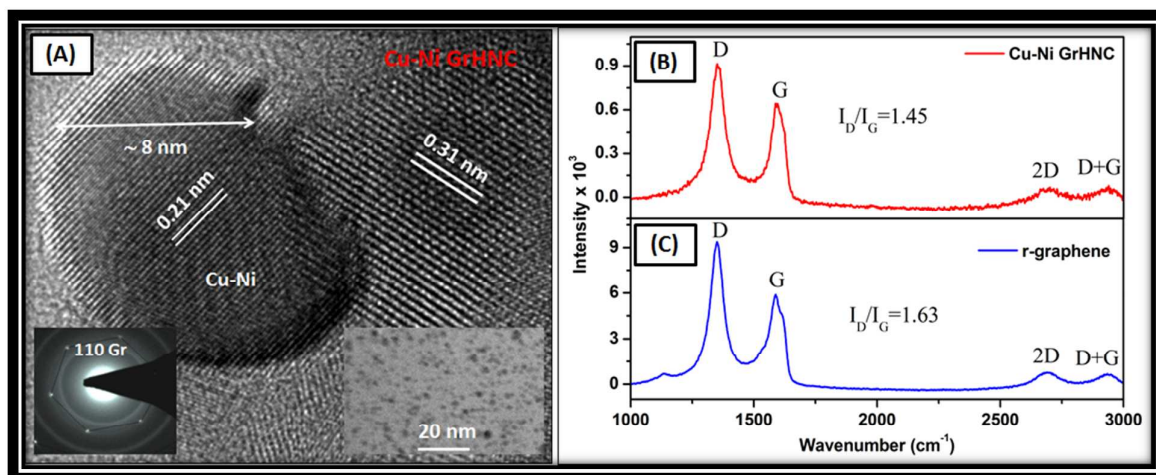
Figure 3: (A) Atomic scale HRTEM images of Cu-Ni GrHNC. Lleft and right insets show SAED patterns and low magnification TEM image, respectively. Raman spectra observed for **(B)** Cu-Ni GrHNC and **(C)** r-graphene

The photo response of Cu-Ni GrHNC is shown in Fig.4. The inset of this shows the I-V curves of r-graphene (blue curve) and Cu-Ni GrHNC (red curve) at room temperature. The linear nature of I-V curves is typical of ohmic behavior and the same is observed for both r-graphene and Cu-Ni GrHNC. A marginal change observed in the linearity of I-V curve indicates that Cu-Ni doped graphene is more metallic than r-graphene. It was observed that Cu-Ni GrHNC exhibits a quick photo-response when illuminated under white light (halogen lamp). The photo-response of biased (5.0V) device was recorded to be ~ 0.27 mA at 2.1 mW/cm^2, which increases to ~ 0.53 mA when the power of halogen lamp is changed to 5.9 mW/cm^2. The origin of photo-current generation, as seen from the photo response (Fig. 4) of Cu-Ni GrHNC, may be attributed to temperature gradient across two different materials, i.e. Cu-Ni alloy and r-graphene, due distinct difference in their thermoelectric coefficients. It has also been reported earlier, that conductive two dimensional honeycomb carbon material is highly photosensitive at metallic contacts[48] when metallic nano-particles are decorated on graphene layers. The photo-thermoelectric response of metal doped graphene through hot carrier transport[49], suggests that graphene-metal contacts are capable of generating a sizeable photocurrent[50].

Other phenomena contributing to photo-current generation are the midgap state band (MGB) and multi excitation generation (MEG)[51]. In graphene, the boundary and electron scattering centers create a defect, which acts as a MGB[52] trapping centers due to quantum confinement. In the first photo-excitation, electrons move to valance band from conduction band. These electrons then return to valance band by Auger recombination and impact

ionization process and thus via this phenomena these electrons transfer excess energy to another electron in valance band, which upon excitation move to conduction band. This multi-excitation process results in generation of more and more secondary electrons. Finally, the generated photo and secondary electrons get trapped in MGB[24] and may contribute as charge carrier for photo-current generation.
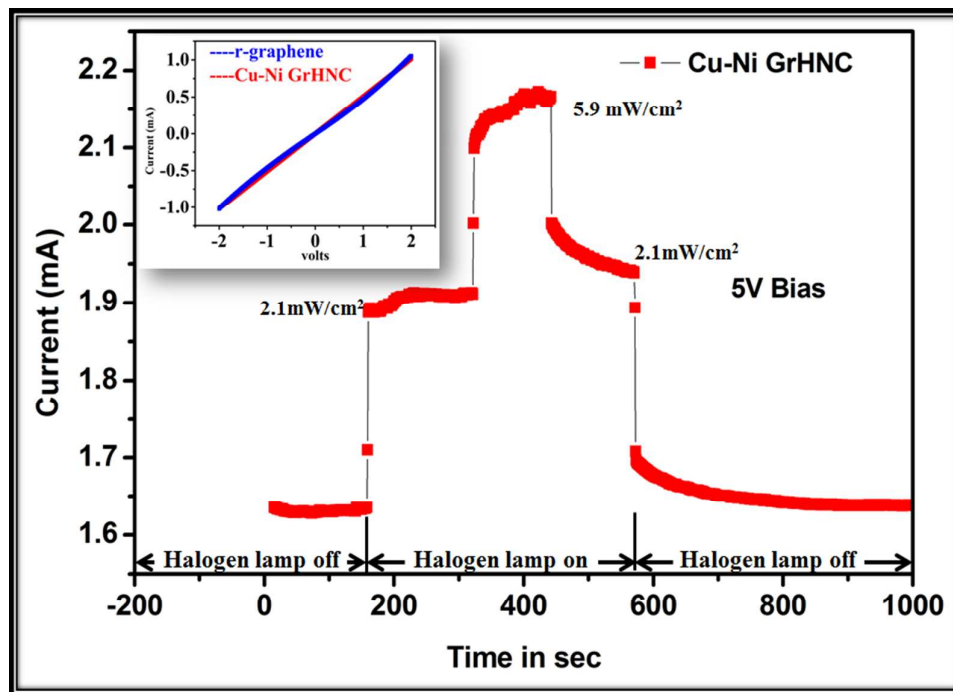
Figure 4: Photocurrent generated by Cu-Ni GrNHC device plotted as a function of time at different powers, 2.1 and 5.9 mW/cm^2, with constant bias voltage (5V). The inset shows I-V characteristics of r-graphene and Cu-Ni GrHNC measured at room temperature.

The response time is an important property of the photodetector performance[53]. The observed growth and decay of photo-current at a constant power of 2.1mW/cm^2 and 5V bias for thin film of Cu-Ni GrHNC are separately plotted in Fig.5 and the corresponding response time is calculated. The growth (Fig.5A) data has been fitted using bi-exponential fitting whereas, mono-exponential fitting[54] is employed for decay (Fig. 5B). The equations used for calculating the growth and decay response time are:

$$I(t) = I_{dark} + A_1 e^{\frac{t}{\tau}} \qquad (1)$$

$$I(t) = I_{dark} + A_2 e^{-\frac{t}{\tau'}} \qquad (2)$$

where I_{dark} denotes dark current; A_1 and A_2 are scaling constant; τ and τ' are growth and decay time constants, respectively, and t refer to observation time when halogen lamp is switched on and off. The decay and growth time constants have been extracted from the experimental data using equation 1 and 2, respectively. The photocurrent growth (Fig. 5A), can be explained by specifying three time constants. Initially, photocurrent rises very fast with time constant $\tau_1 = 0.84$ sec followed by relatively slow growth ($\tau_2 = 31.73$ sec). Later, the photocurrent increases negligibly and appears to saturate. As the power is switched off, a quick decay in current (to $1/e^{th}$ of its initial value) has been observed with $\tau'_1 = 2.22$ sec, which further decays slowly ($\tau'_2 = 93.19$ sec).
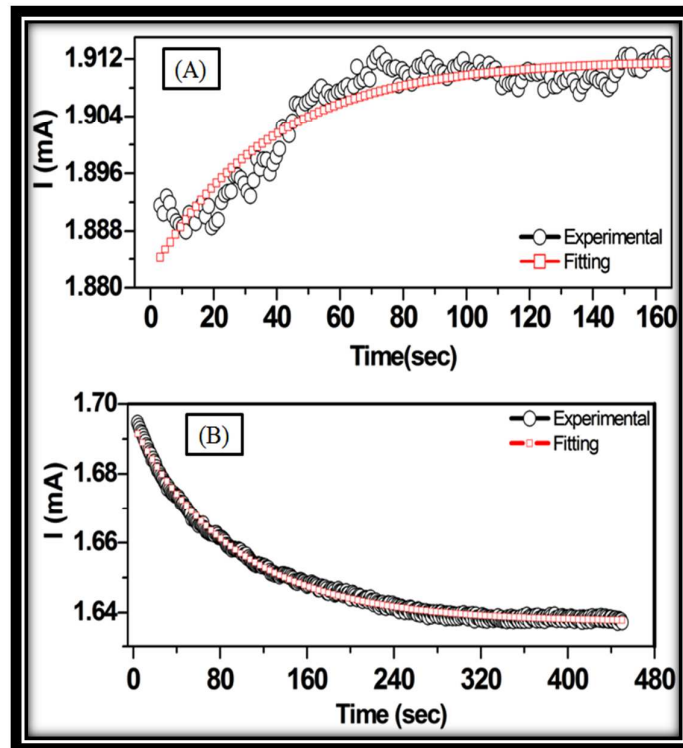
Figure 5: **(A)** Measured growth of photocurrent as a function of time when Cu-Ni GrNHC device was illuminated with 2.1 mW/cm^2 power along with its bi-exponential fitting **(B)** measured decay of photocurrent as the power is switched off; the experimental data was fitted using mono-exponential fitting

The growth time constant (τ_1) is found to be less than decay time constant (τ'_1), which may be due to the electrons trapped in MGB and multi excitation process. We hypothesize that the photo-thermoelectric phenomenon may also be responsible, where temperature gradient is generated between graphene and metal nano-particles. Several studies support the fact that graphene p-n junction works as a photodetector[55]. The photo-response is found to depend on the generation of secondary photo-emission by Cu-Ni nano-particles produced via photo-thermoelectric effect[56] and multiple electron-hole pair generation in graphene by single photonic excitation[30, 51]. It has been observed that the photo-thermoelectric effect may provide an useful insight to the majority charge carriers in Cu-Ni nano-particle decorated hybrid graphene based nano-composite. However, the entire network of Cu-Ni GrHNC, fabricated in the present study, behaves as a p-n junction at metal-graphene contacts exhibiting an enhanced photocurrent generation and a quick response time, making it a suitable candidate for future photovoltaic applications[31].

4. Conclusion

We report the synthesis of Cu-Ni reduced graphene hybrid nano-composite by employing a simple reduction chemistry process, which is quick and economical. The microscopy results of synthesized r-graphene nano-layers confirmed a graphene honeycomb network. The decoration of Cu-Ni nano-particles on r-graphene via chemical route show uniform distribution. The electrical properties exhibit an ohmic behavior of Cu-Ni reduced graphene

hybrid nano-composite and exhibited photosensitive response. The hybrid nano-composite is found to be sensitive towards photon to electron conversion and total current variation of 0.537 mA has been measured. The photocurrent grows with time constant τ_1=0.83sec which is less than initial decay time constant, τ'_2= 2.22sec, indicating superior light absorption and long life time of device. Owing to the structure and improved properties it is suggested that Cu-Ni nanoparticles decorated r-graphene hybrid nano-layers could be a promising material for energy harvesting devices.

Acknowledgements

References:

1. F. Bonaccorso, Z. Sun, T. Hasan and A. C. Ferrari, *Nat Photon*, 2010, **4**, 611-622.
2. P. Avouris, *Nano Letters*, 2010, **10**, 4285-4294.
3. R. R. Nair, P. Blake, A. N. Grigorenko, K. S. Novoselov, T. J. Booth, T. Stauber, N. M. R. Peres and A. K. Geim, *Science*, 2008, **320**, 1308.
4. C. Berger, Z. Song, X. Li, X. Wu, N. Brown, C. Naud, D. Mayou, T. Li, J. Hass, A. N. Marchenkov, E. H. Conrad, P. N. First and W. A. de Heer, *Science*, 2006, **312**, 1191-1196.
5. A. A. Balandin, S. Ghosh, W. Bao, I. Calizo, D. Teweldebrhan, F. Miao and C. N. Lau, *Nano Letters*, 2008, **8**, 902-907.
6. M. Gullans, D. E. Chang, F. H. L. Koppens, F. J. G. de Abajo and M. D. Lukin, *Physical Review Letters*, 2013, **111**, 247401.
7. Y. Liu, R. Cheng, L. Liao, H. Zhou, J. Bai, G. Liu, L. Liu, Y. Huang and X. Duan, *Nature communications*, 2011, **2**, 579.
8. Y. Liu, B. Xie, Z. Zhang, Q. Zheng and Z. Xu, *Journal of the Mechanics and Physics of Solids*, 2012, **60**, 591-605.
9. Y. Zhu, S. Murali, M. D. Stoller, K. J. Ganesh, W. Cai, P. J. Ferreira, A. Pirkle, R. M. Wallace, K. A. Cychosz, M. Thommes, D. Su, E. A. Stach and R. S. Ruoff, *Science*, 2011, **332**, 1537-1541.
10. G. Wang, X. Shen, J. Yao and J. Park, *Carbon*, 2009, **47**, 2049-2053.

11.   T. T. Baby, S. S. J. Aravind, T. Arockiadoss, R. B. Rakhi and S. Ramaprabhu, *Sensors and Actuators B: Chemical*, 2010, **145**, 71-77.

12.   Y. Huang, X. Dong, Y. Shi, C. M. Li, L.-J. Li and P. Chen, *Nanoscale*, 2010, **2**, 1485-1488.

13.   X. Yang, Y. Wang, X. Huang, Y. Ma, Y. Huang, R. Yang, H. Duan and Y. Chen, *Journal of Materials Chemistry*, 2011, **21**, 3448-3454.

14.   X. Yang, X. Zhang, Y. Ma, Y. Huang, Y. Wang and Y. Chen, *Journal of Materials Chemistry*, 2009, **19**, 2710-2714.

15.   G. Eda and M. Chhowalla, *Advanced Materials*, 2010, **22**, 2392-2415.

16.   Z. Chen, C. Xu, C. Ma, W. Ren and H.-M. Cheng, *Advanced Materials*, 2013, **25**, 1296-1300.

17.   G. Lu, K. Yu, Z. Wen and J. Chen, *Nanoscale*, 2013, **5**, 1353-1368.

18.   S. Y. Zhou, G. H. Gweon, A. V. Fedorov, P. N. First, W. A. de Heer, D. H. Lee, F. Guinea, A. H. Castro Neto and A. Lanzara, *Nat Mater*, 2007, **6**, 770-775.

19.   C. Xu, X. Wang and J. Zhu, *The Journal of Physical Chemistry C*, 2008, **112**, 19841-19845.

20.   S. Deng, V. Tjoa, H. M. Fan, H. R. Tan, D. C. Sayle, M. Olivo, S. Mhaisalkar, J. Wei and C. H. Sow, *Journal of the American Chemical Society*, 2012, **134**, 4905-4917.

21.   X. Wang, X. Zhou, K. Yao, J. Zhang and Z. Liu, *Carbon*, 2011, **49**, 133-139.

22.   C. Zhang, X. Peng, Z. Guo, C. Cai, Z. Chen, D. Wexler, S. Li and H. Liu, *Carbon*, 2012, **50**, 1897-1903.

23.   A. Kongkanand, K. Tvrdy, K. Takechi, M. Kuno and P. V. Kamat, *Journal of the American Chemical Society*, 2008, **130**, 4007-4015.

24.   B. Y. Zhang, T. Liu, B. Meng, X. Li, G. Liang, X. Hu and Q. J. Wang, *Nat Commun*, 2013, **4**, 1811.

25.   D. Shao, M. Yu, H. Sun, T. Hu, J. lian and S. Sawyer, *Nanoscale*, 2013, **5**, 3664-3667.

26.   Y. Liu, R. Cheng, L. Liao, H. Zhou, J. Bai, G. Liu, L. Liu, Y. Huang and X. Duan, *Nat Commun*, 2011, **2**, 579.

27.   T. J. Echtermeyer, L. Britnell, P. K. Jasnos, A. Lombardo, R. V. Gorbachev, A. N. Grigorenko, A. K. Geim, A. C. Ferrari and K. S. Novoselov, *Nat Commun*, 2011, **2**, 458.

28.   W. Li, Y. He, L. Wang, G. Ding, Z.-Q. Zhang, R. W. Lortz, P. Sheng and N. Wang, *Physical Review B*, 2011, **84**, 045431.

29.   J. Zhu, Q. H. Liu and T. Lin, *Nanoscale*, 2013, **5**, 7785-7789.

30.   K. J. Tielrooij, J. C. W. Song, S. A. Jensen, A. Centeno, A. Pesquera, A. Zurutuza Elorza, M. Bonn, L. S. Levitov and F. H. L. Koppens, *Nat Phys*, 2013, **9**, 248-252.

31.   M. C. Lemme, F. H. L. Koppens, A. L. Falk, M. S. Rudner, H. Park, L. S. Levitov and C. M. Marcus, *Nano Letters*, 2011, **11**, 4134-4137.

32.   Z. Jarrahi, Y. Cao, T. Hong, Y. S. Puzyrev, B. Wang, J. Lin, A. H. Huffstutter, S. T. Pantelides and Y.-Q. Xu, *Nanoscale*, 2013, **5**, 12206-12211.

33.   N. M. Gabor, J. C. W. Song, Q. Ma, N. L. Nair, T. Taychatanapat, K. Watanabe, T. Taniguchi, L. S. Levitov and P. Jarillo-Herrero, *Science*, 2011, **334**, 648-652.

34.   H. Sevinçli and G. Cuniberti, *Physical Review B*, 2010, **81**, 113401.

35.   H. Zhang, G. Lee and K. Cho, *Physical Review B*, 2011, **84**, 115460.

36.   J.-W. Jiang, B.-S. Wang and J.-S. Wang, *Applied Physics Letters*, 2011, **98**, -.

37.   J. H. Chen, C. Jang, S. Adam, M. S. Fuhrer, E. D. Williams and M. Ishigami, *Nat Phys*, 2008, **4**, 377-381.

38.   N. Toshima and T. Yonezawa, *New Journal of Chemistry*, 1998, **22**, 1179-1201.

39.   R. G. Delatorre, M. L. Sartorelli, A. Q. Schervenski, A. A. Pasa and S. Güths, *Journal of Applied Physics*, 2003, **93**, 6154-6158.

40.   Z. Xu and M. J. Buehler, *Journal of Physics: Condensed Matter*, 2010, **22**, 485301.

41.   P.-G. Ren, D.-X. Yan, X. Ji, T. Chen and Z.-M. Li, *Nanotechnology*, 2011, **22**, 055705.

42.   L. J. Cote, J. Kim, Z. Zhang, C. Sun and J. Huang, *Soft Matter*, 2010, **6**, 6096-6101.

43.   S. Ghosh, B. K. Sarker, A. Chunder, L. Zhai and S. I. Khondaker, *Applied Physics Letters*, 2010, **96**, -.

44. H. C. Schniepp, J.-L. Li, M. J. McAllister, H. Sai, M. Herrera-Alonso, D. H. Adamson, R. K. Prud'homme, R. Car, D. A. Saville and I. A. Aksay, *The Journal of Physical Chemistry B*, 2006, **110**, 8535-8539.
45. I. Baskaran, T. S. N. Sankara Narayanan and A. Stephen, *Materials Letters*, 2006, **60**, 1990-1995.
46. M. R. Karim, H. Shinoda, M. Nakai, K. Hatakeyama, H. Kamihata, T. Matsui, T. Taniguchi, M. Koinuma, K. Kuroiwa, M. Kurmoo, Y. Matsumoto and S. Hayami, *Advanced Functional Materials*, 2013, **23**, 323-332.
47. D.-K. Lim, A. Barhoumi, R. G. Wylie, G. Reznor, R. S. Langer and D. S. Kohane, *Nano Letters*, 2013, **13**, 4075-4079.
48. W. J. Yu, Y. Liu, H. Zhou, A. Yin, Z. Li, Y. Huang and X. Duan, *Nat Nano*, 2013, **8**, 952-958.
49. J. C. W. Song, M. S. Rudner, C. M. Marcus and L. S. Levitov, *Nano Letters*, 2011, **11**, 4688-4692.
50. J. Park, Y. H. Ahn and C. Ruiz-Vargas, *Nano Letters*, 2009, **9**, 1742-1746.
51. T. Winzer, A. Knorr and E. Malic, *Nano Letters*, 2010, **10**, 4839-4843.
52. J.-H. Chen, W. G. Cullen, C. Jang, M. S. Fuhrer and E. D. Williams, *Physical Review Letters*, 2009, **102**, 236805.
53. P. Hu, Z. Wen, L. Wang, P. Tan and K. Xiao, *ACS Nano*, 2012, **6**, 5988-5994.
54. J. Sun, L. Xiao, D. Meng, J. Geng and Y. Huang, *Chemical Communications*, 2013, **49**, 5538-5540.
55. E. C. Peters, E. J. H. Lee, M. Burghard and K. Kern, *Applied Physics Letters*, 2010, **97**, -.
56. D. Basko, *Science*, 2011, **334**, 610-611.